

Naphthalimide based Smart Sensor for $\text{CN}^-/\text{Fe}^{3+}$ and H_2S . Synthesis and Application in RAW264.7 cell and Zebrafish Imaging

Sanay Naha^a, Shu-Pao Wu^{b*}, and Sivan Velmathi^{a*}

^aOrganic and Polymer Synthesis Laboratory, Department of Chemistry, National Institute of Technology, Tiruchirappalli, India

^bDepartment of Applied Chemistry, National Chiao Tung University, Hsinchu, Taiwan.

Email: velmathis@nitt.edu, spwu@mail.nctu.edu.tw

Content of Supporting Information:

Fig. S1: IR-spectrum of receptor R.

Fig. S2: ^1H -NMR spectrum of receptor R in DMSO-d_6 .

Fig. S3: ^{13}C -NMR spectrum of receptor R in DMSO-d_6 .

Fig. S4: HR-Mass spectrum of receptor R.

Fig. S5: Solvent effect on receptor and its cyanide sensing.

Fig. S6: Images of anion selectivity and UV-PL spectrum in only DMSO solvent.

Fig. S7: Effect of water content in cyanide selectivity by receptor.

Fig. S8: **Fig. S8:** (a) Naked eye colour change and (b) under UV-light turn-on emission for CN^- among CN^- , NO_2^- , S^{2-} , ClO^- , and HSO_3^- in 5% water-DMSO medium; (c) Electronic and (d) emission spectra for optical selectivity of CN^- ; (e) Naked eye image and (f) electronic spectrum of the of receptor R with $\text{S}_2\text{O}_4^{2-}$, HSO_3^- and HSO_4^- .

Fig. S9: Interference studies for cyanide sensing by receptor against competing anions.

Fig. S10: (a) Job's plot of CN^- detection by receptor and (b) Job's plot of Fe^{3+} detection by receptor + CN^- .

Fig. S11: (a) Binding constant and (b) Limit of detection of CN^- by receptor R.

Fig. S12: (a) Binding constant and (b) Limit of detection of Fe^{3+} by R+ CN^- .

Fig. S13: Limit of detection of H_2S by receptor R.

Fig. 14: Strip Test for CN^- (a) Under UV-Light and naked eye response of the probe R with various concentration of CN^- ranging from (0.1-10) μM ; Strip test for H_2S (b) Naked eye response of the probe R with various concentration of H_2S ranging from (0.1-10) μM .

Table S1: Comparison table of the reported receptors for CN^- , Fe^{3+} , and H_2S .

Table S2: Quantum Yield of the $\text{CN}^-/\text{Fe}^{3+}$ relay sensing process.

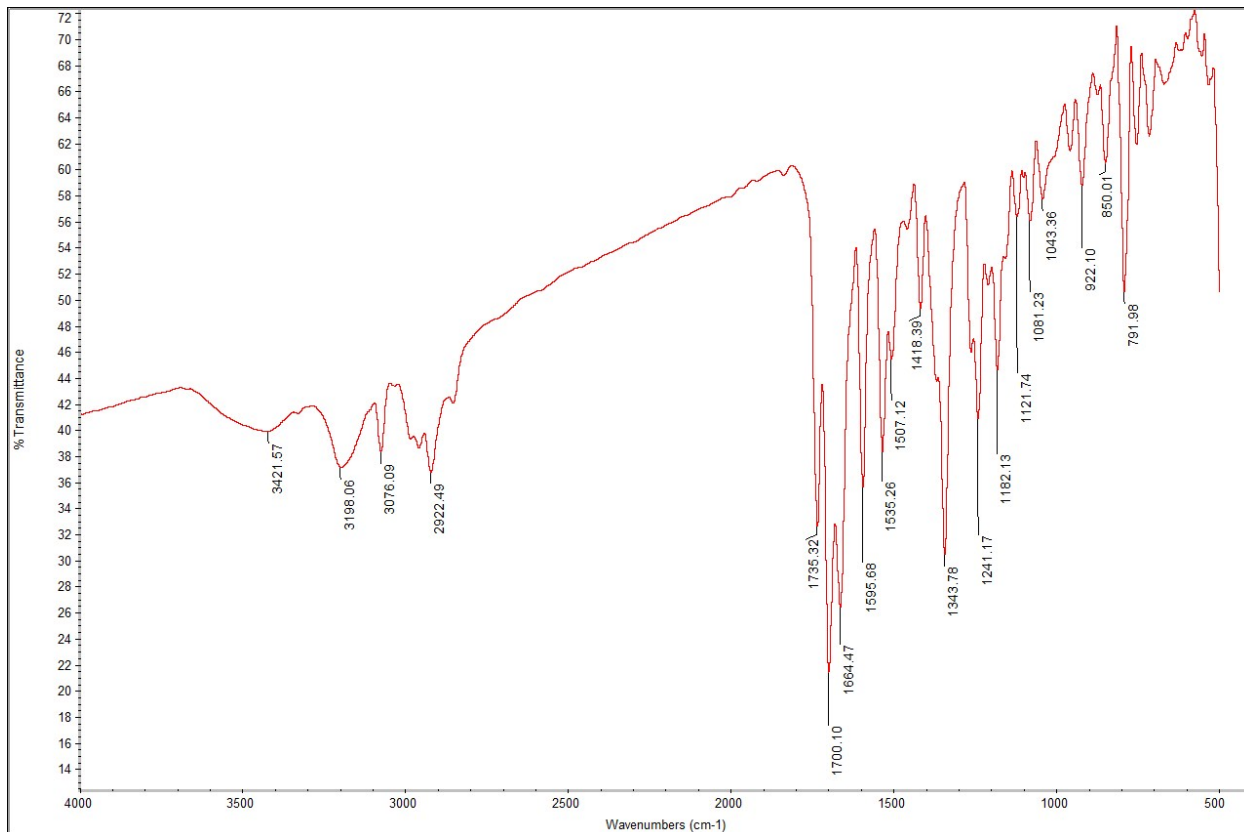


Fig. S1: IR-spectrum of receptor R.

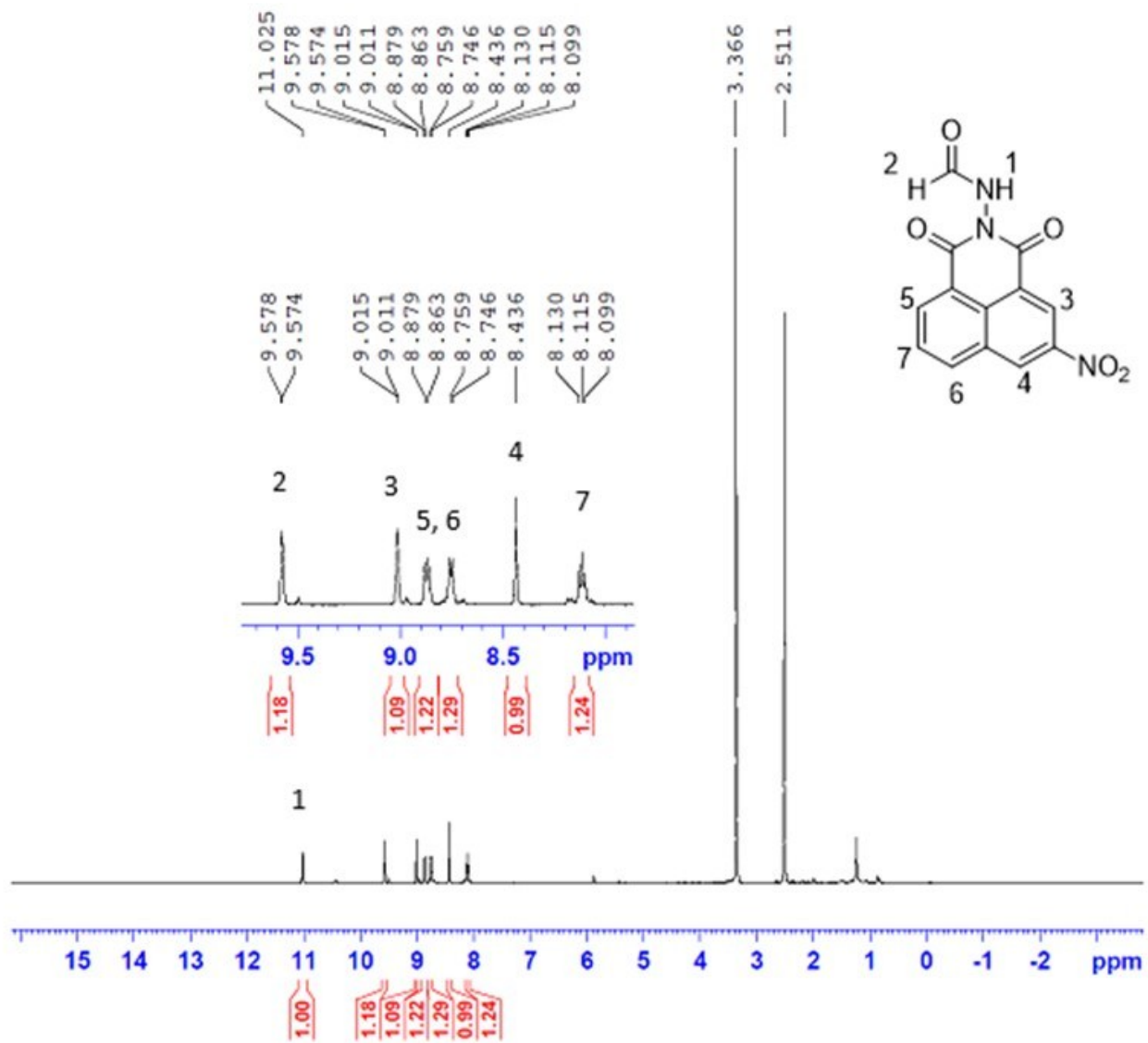
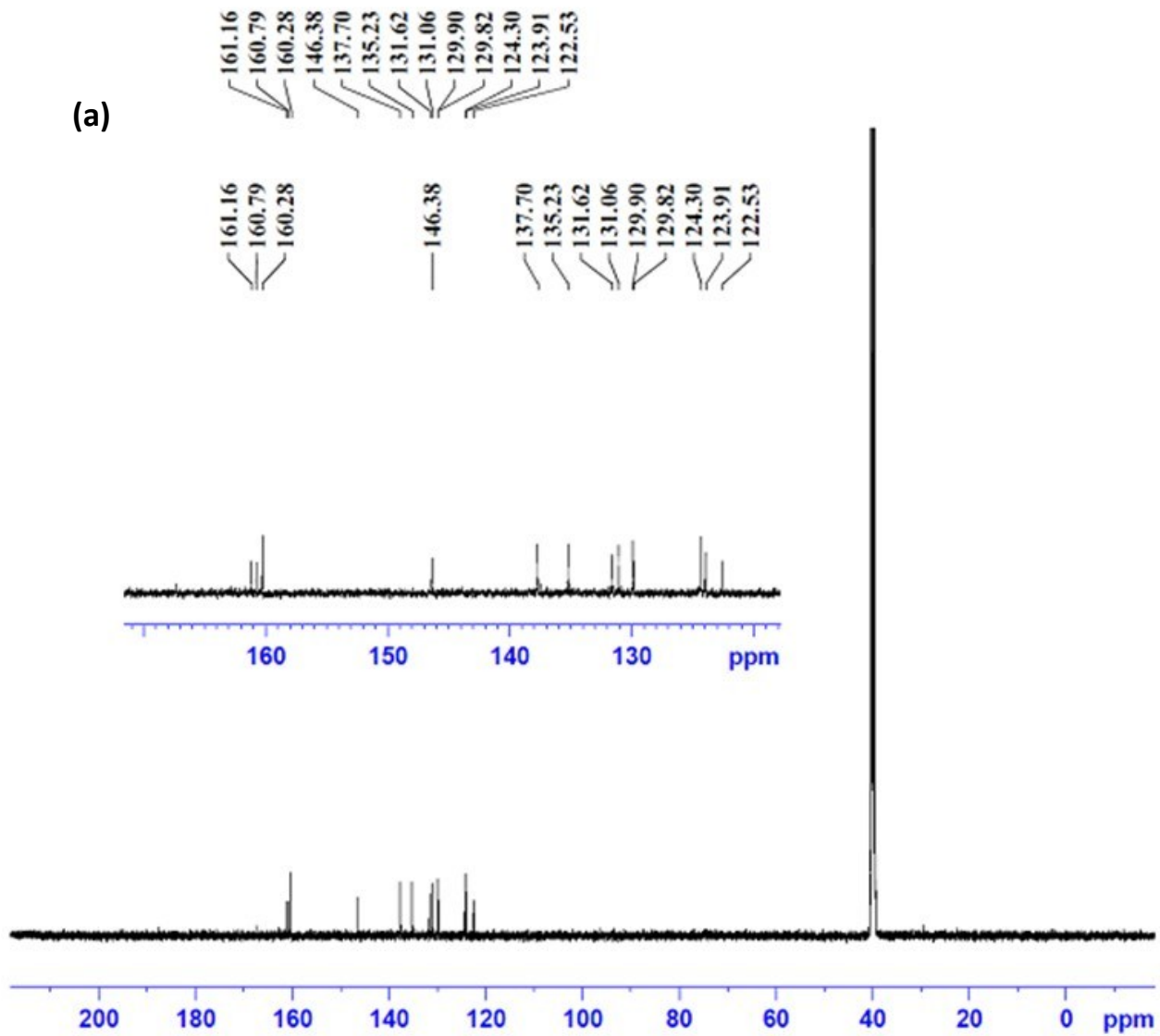
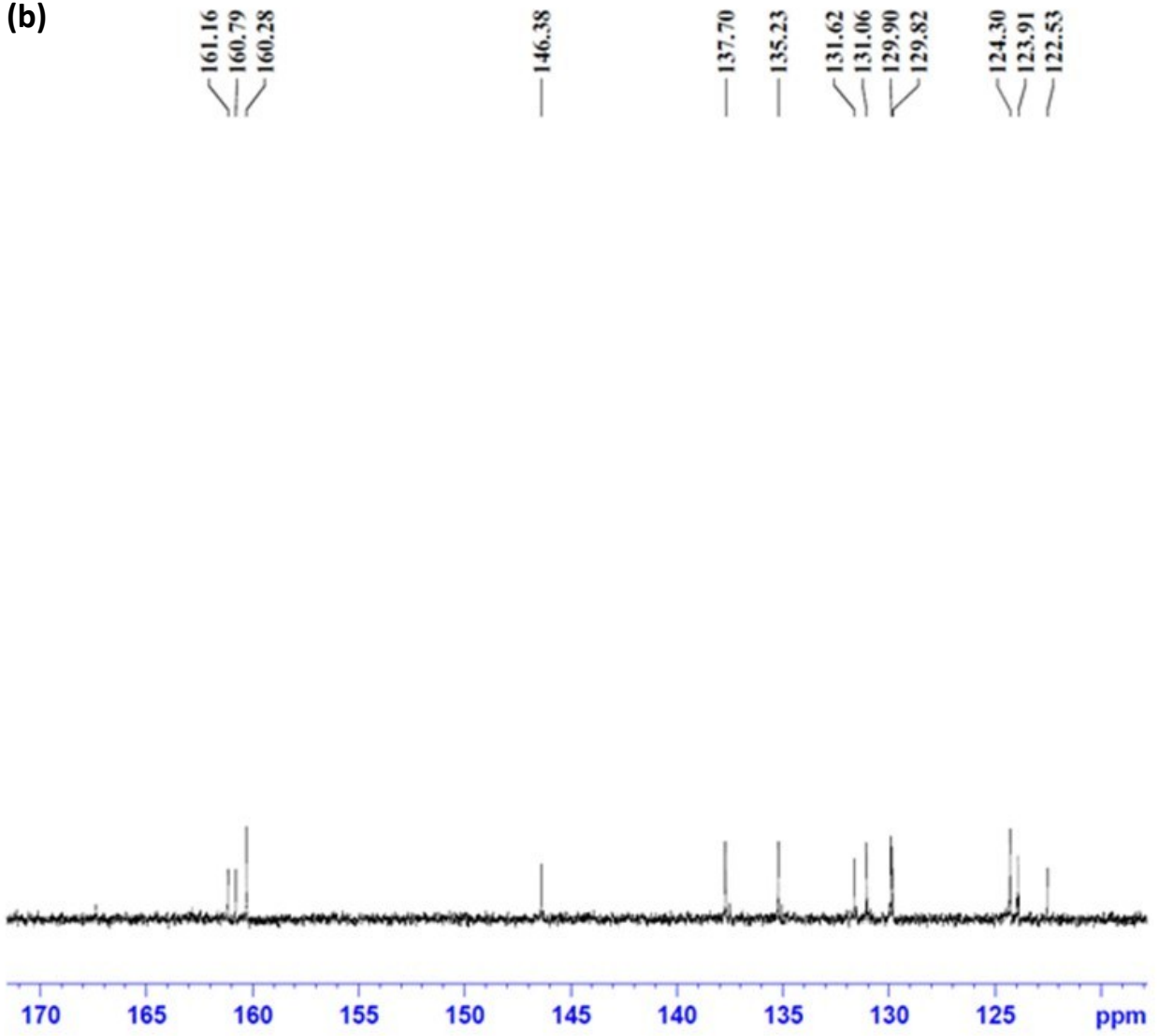


Fig. S2: $^1\text{H-NMR}$ spectrum of receptor R in DMSO-d_6 .

(a)



(b)



(c)

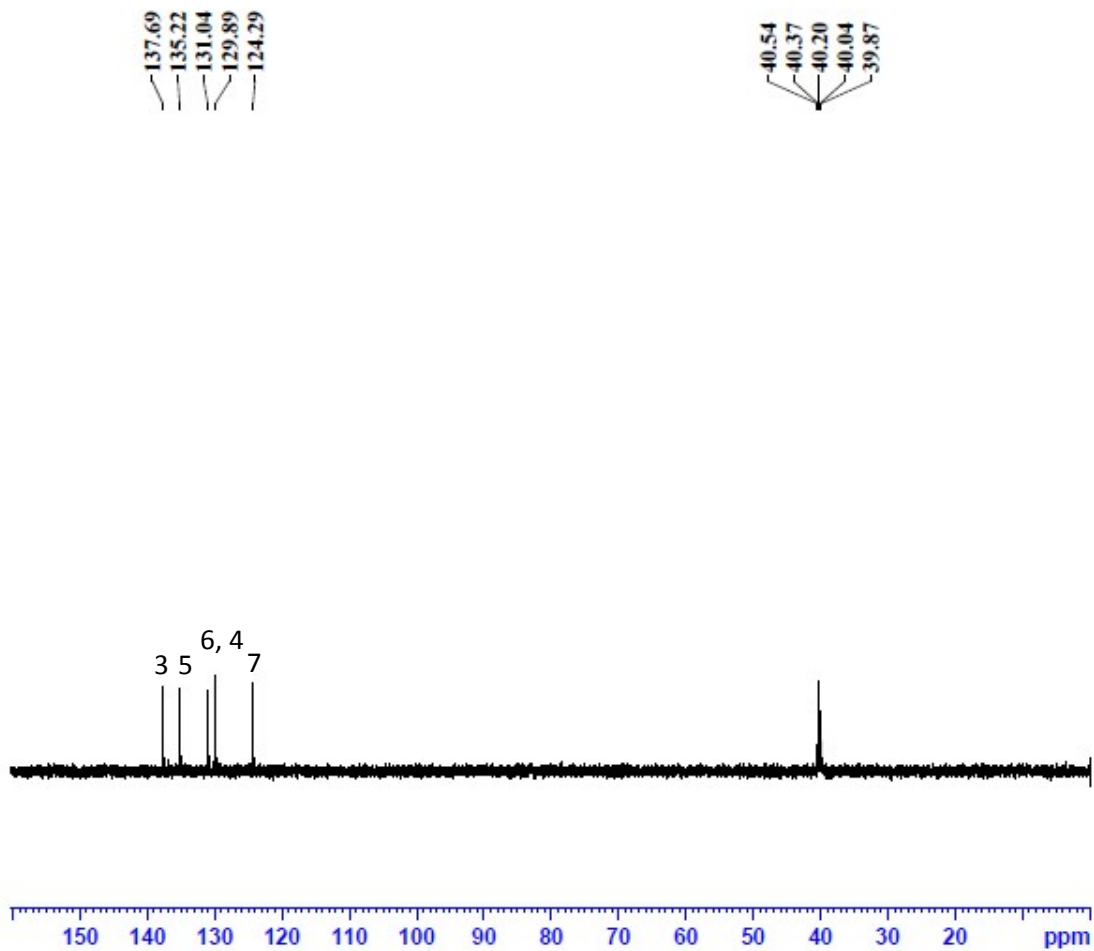


Fig. S3: (a) ^{13}C -NMR spectrum of receptor R, (b) Expansion of ^{13}C -NMR spectrum of the receptor R from 120 ppm to 180 ppm and (c) $^{135}\text{DEPT}$ -NMR spectrum of the receptor R in DMSO-d_6 .

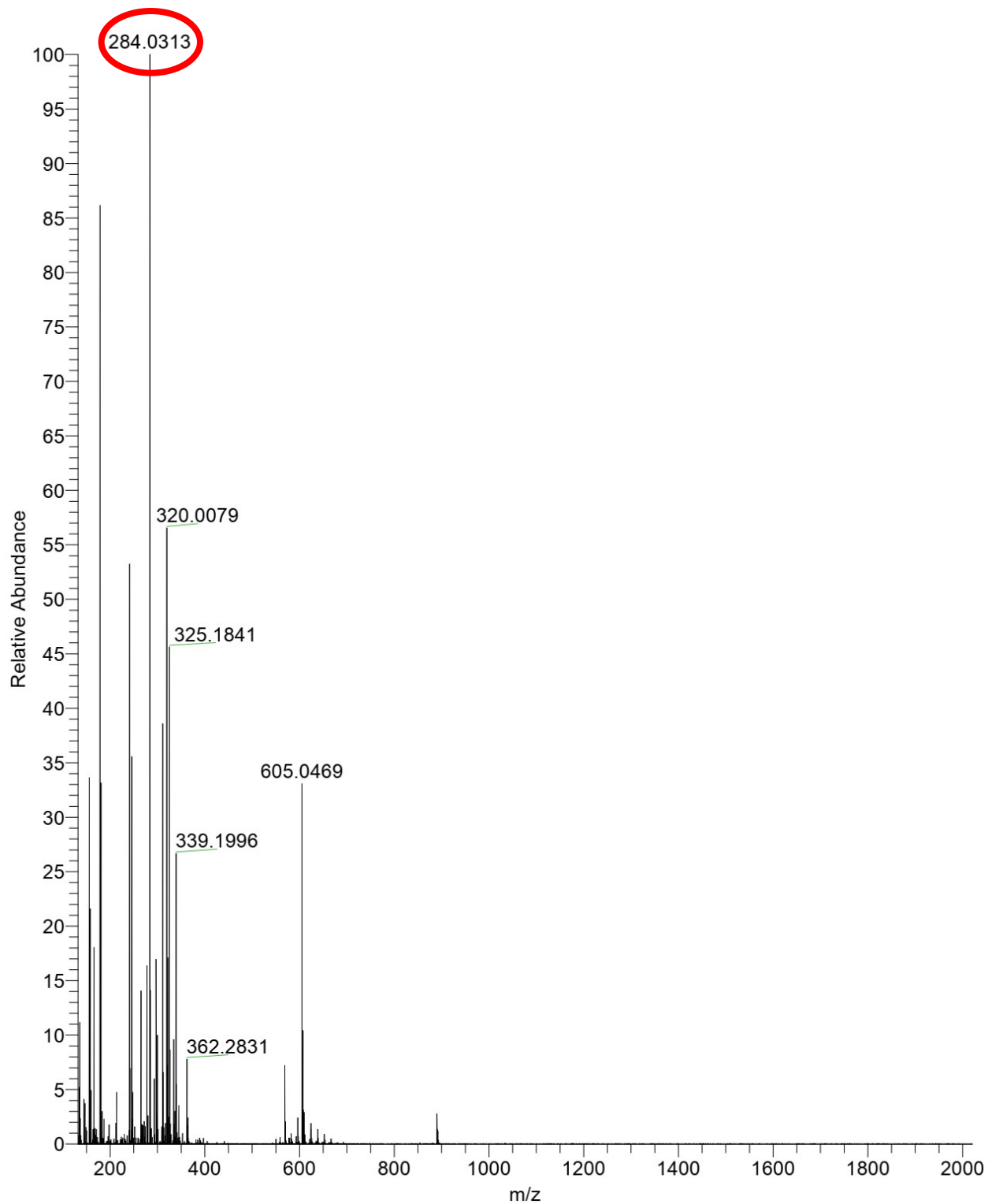


Fig. S4: HR-Mass spectrum of receptor R.

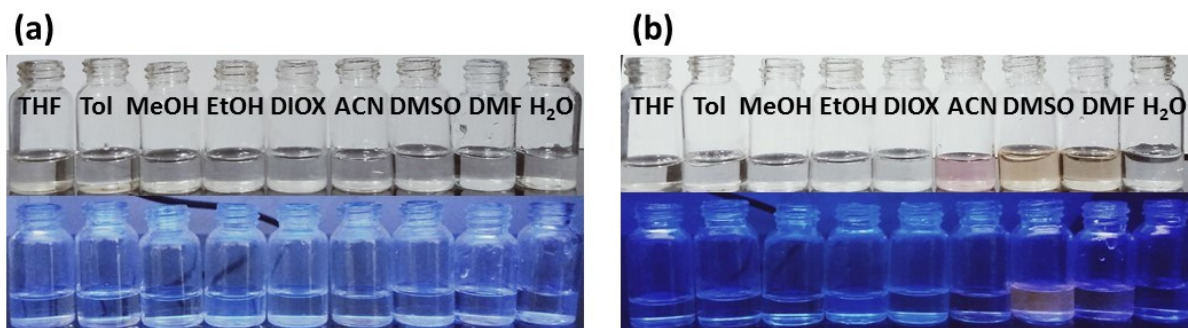


Fig. S5: Solvent effect on receptor and its cyanide sensing. (a) Naked eye and under UV light Images of only receptor and (b) naked eye and under UV light Images of receptor with cyanide in various solvents.

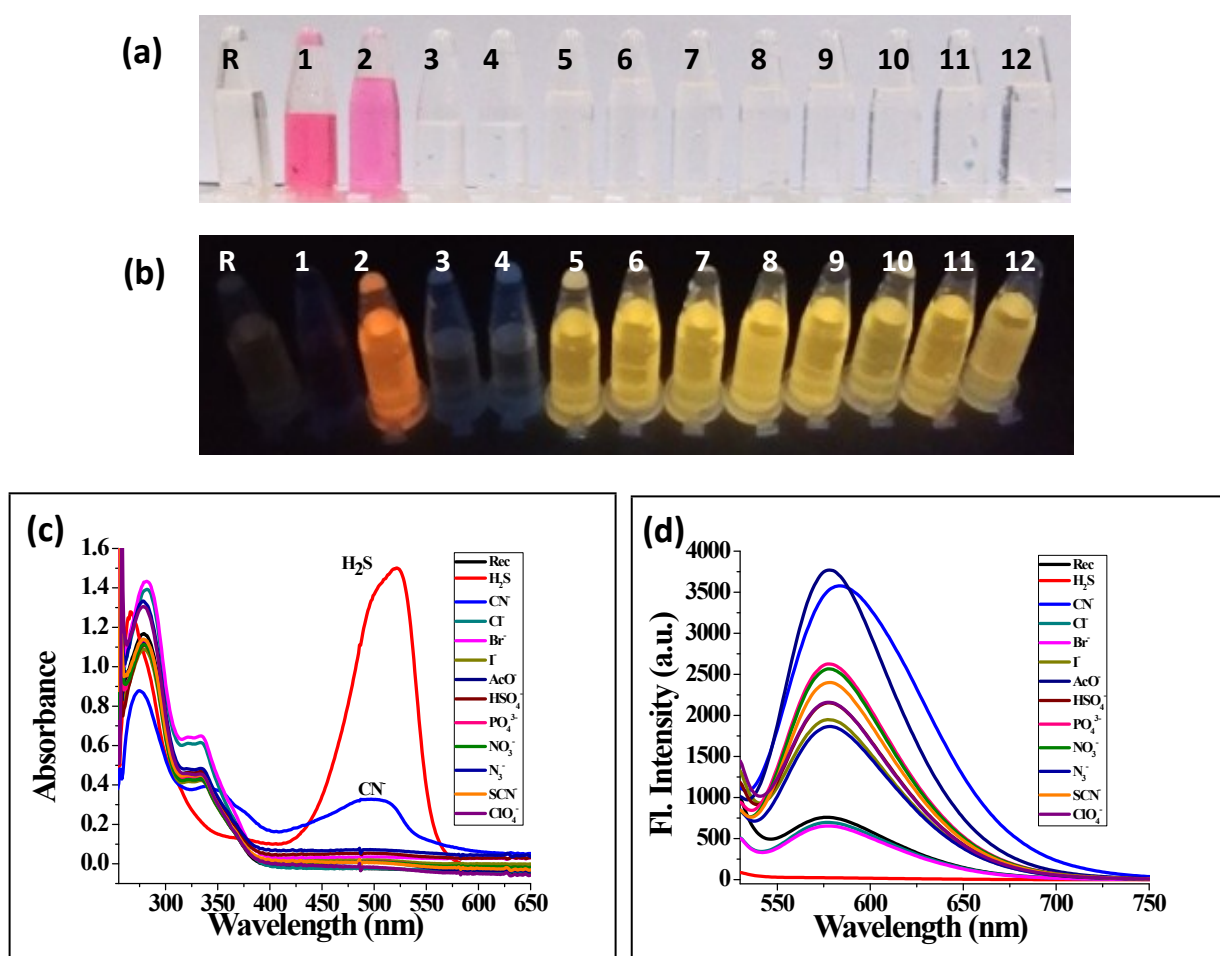


Fig. S6: Images of anion selectivity and UV-PL spectrum in only DMSO solvent. (a) Naked eye colour change and (b) under UV-light; (c) the electronic and (d) emission responses of the receptor with all anions in only DMSO solvent. Where 1= H₂S, 2= CN⁻, 3= Cl⁻, 4= Br⁻, 5= I⁻, 6= AcO⁻, 7= HSO₄⁻, 8= PO₄³⁻, 9= NO₃⁻, 10= N₃⁻, 11= SCN⁻, and 12= ClO₄⁻.

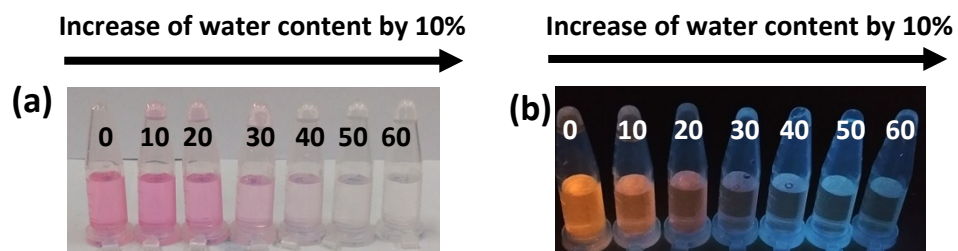


Fig. S7: Effect of water content in cyanide selectivity by receptor. (a) Naked eye and (b) under UV light images of water effect in cyanide response.

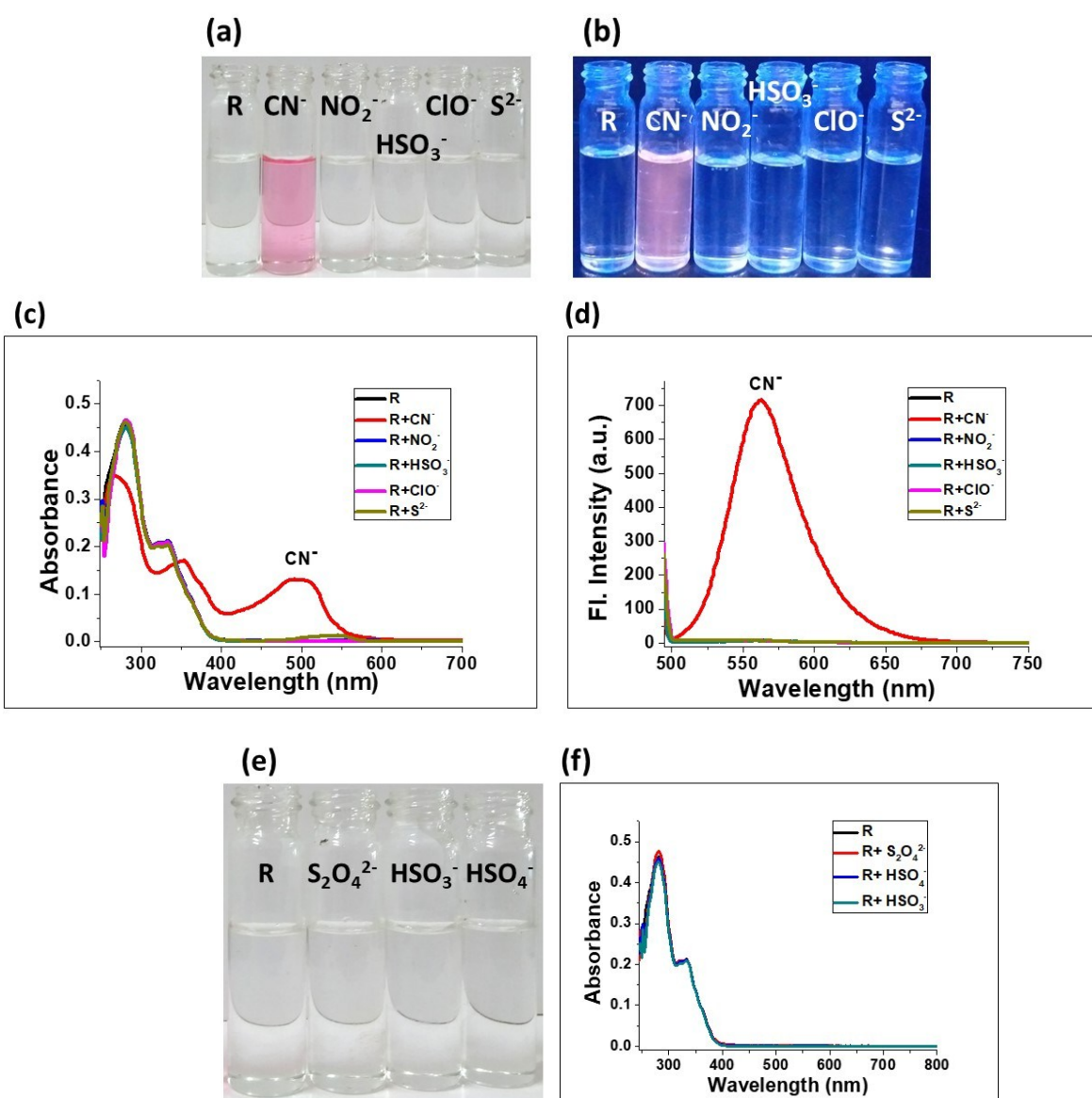


Fig. S8: (a) Naked eye colour change and (b) under UV-light turn-on emission for CN^- among CN^- , NO_2^- , S^{2-} , ClO^- , and HSO_3^- in 5% water-DMSO medium; (c) Electronic and (d) emission spectra for optical selectivity of CN^- ; (e) Naked eye image and (f) electronic spectrum of the of receptor **R** with $\text{S}_2\text{O}_4^{2-}$, HSO_3^- and HSO_4^- .

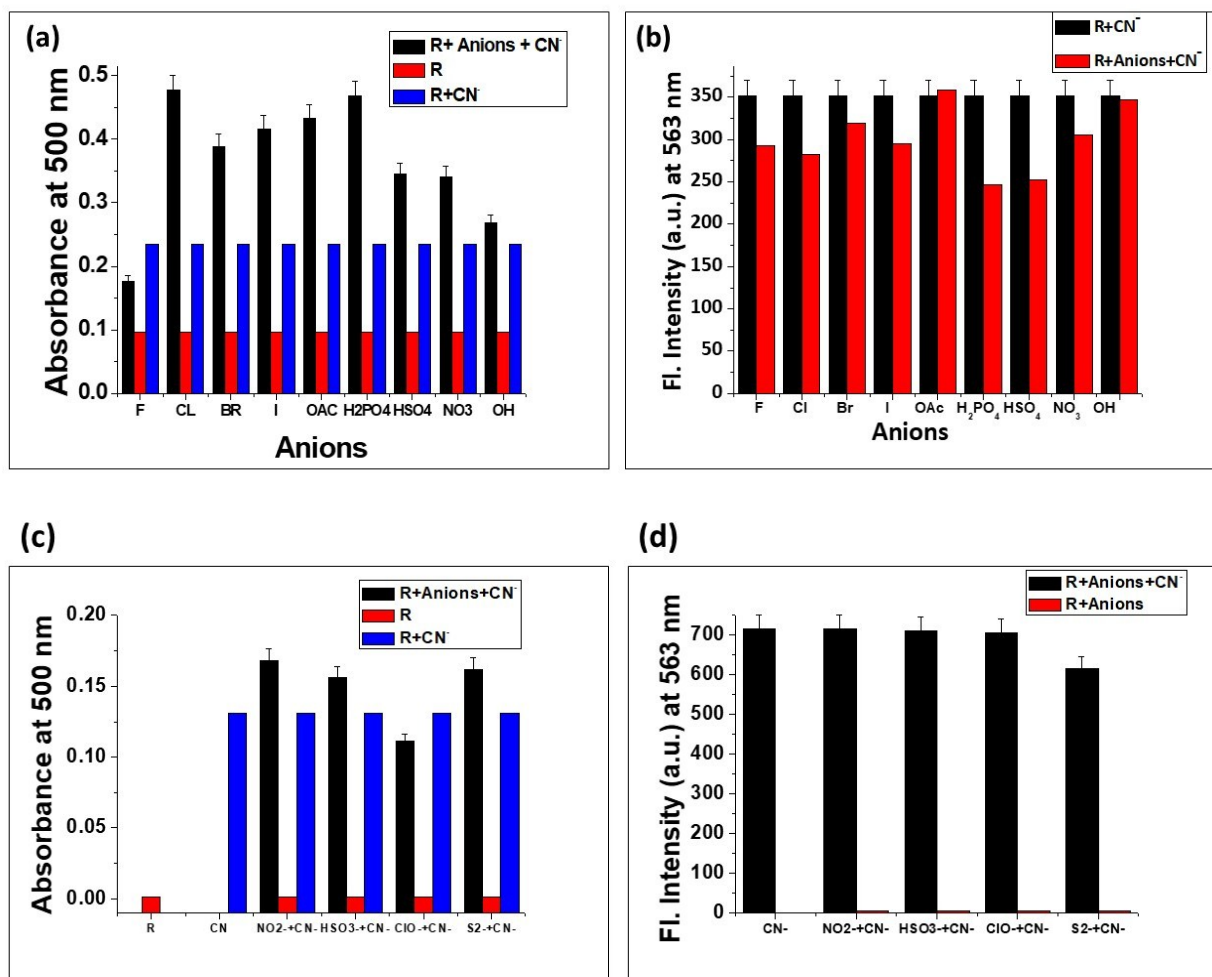


Fig. S9: Interference studies for cyanide sensing by receptor against competing anions. Comparison of (a) electronic response at 500 nm and (b) emission response at 563 nm in presence of other competing anions; (c) Electronic and (d) emission spectra for interference studies of the anions on cyanide selectivity among CN^- , NO_2^- , S^{2-} , ClO^- , and HSO_3^- .

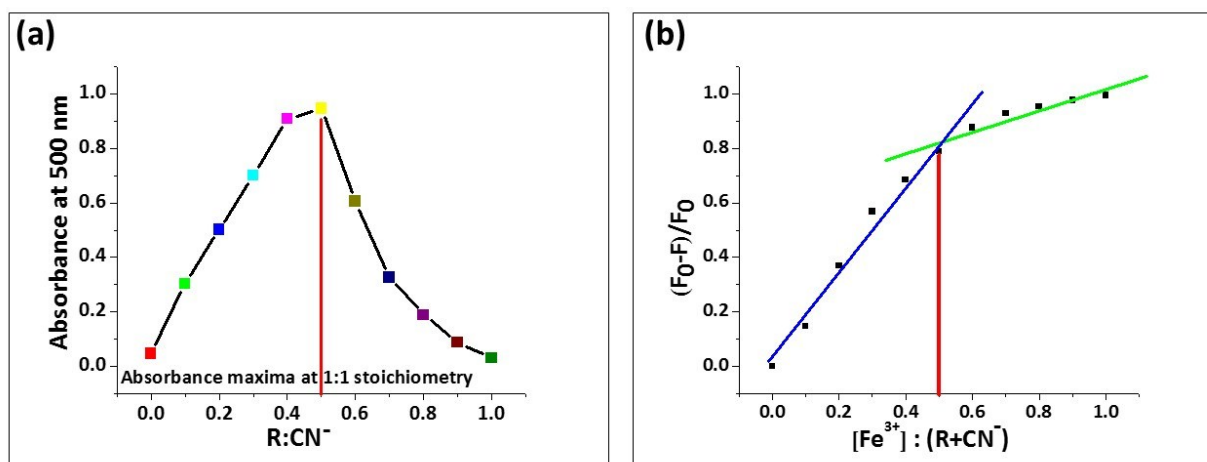


Fig. S10: (a) Job's plot of CN⁻ detection by receptor and (b) Job's plot of Fe³⁺ detection by receptor+CN⁻.

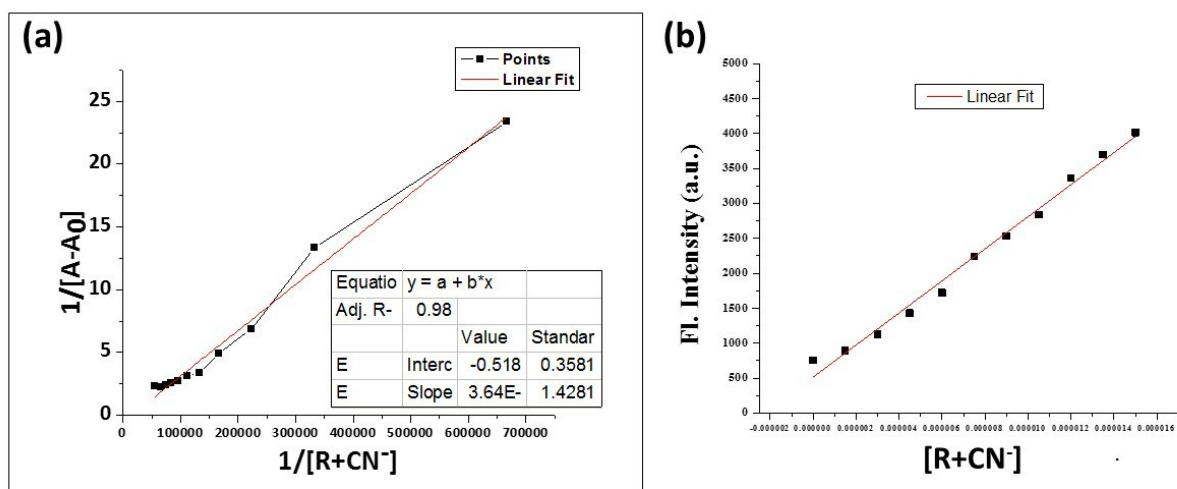


Fig. S11: (a) Binding constant and (b) Limit of detection of CN⁻ by receptor R.

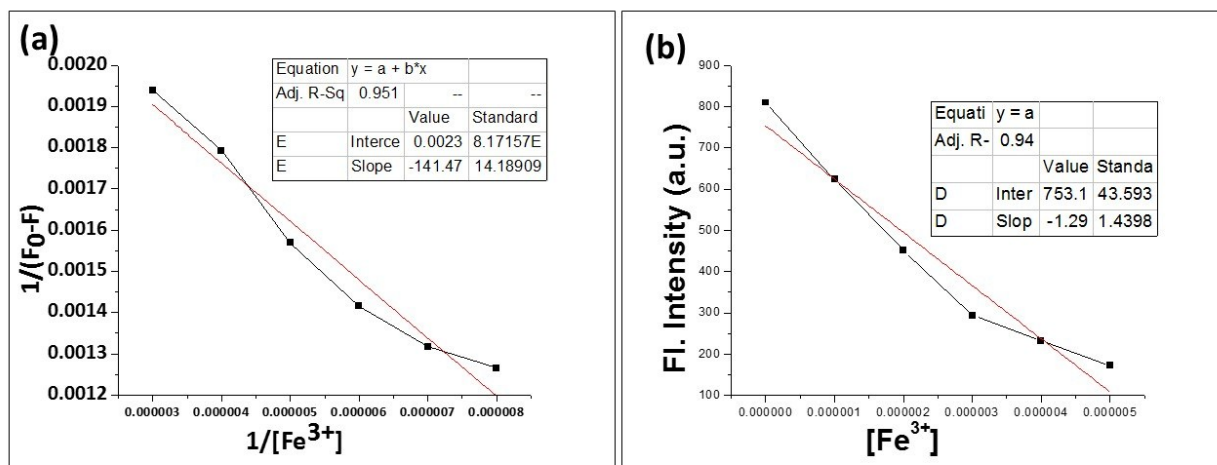


Fig. S12: (a) Binding constant and (b) Limit of detection of Fe^{3+} by $\text{R}+\text{CN}^-$.

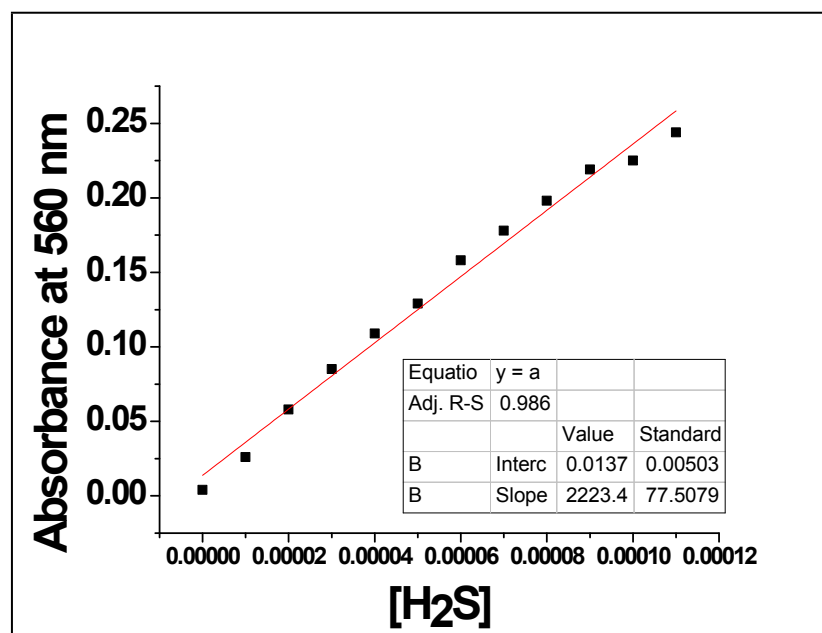


Fig. S13: Limit of detection of H_2S by receptor R.

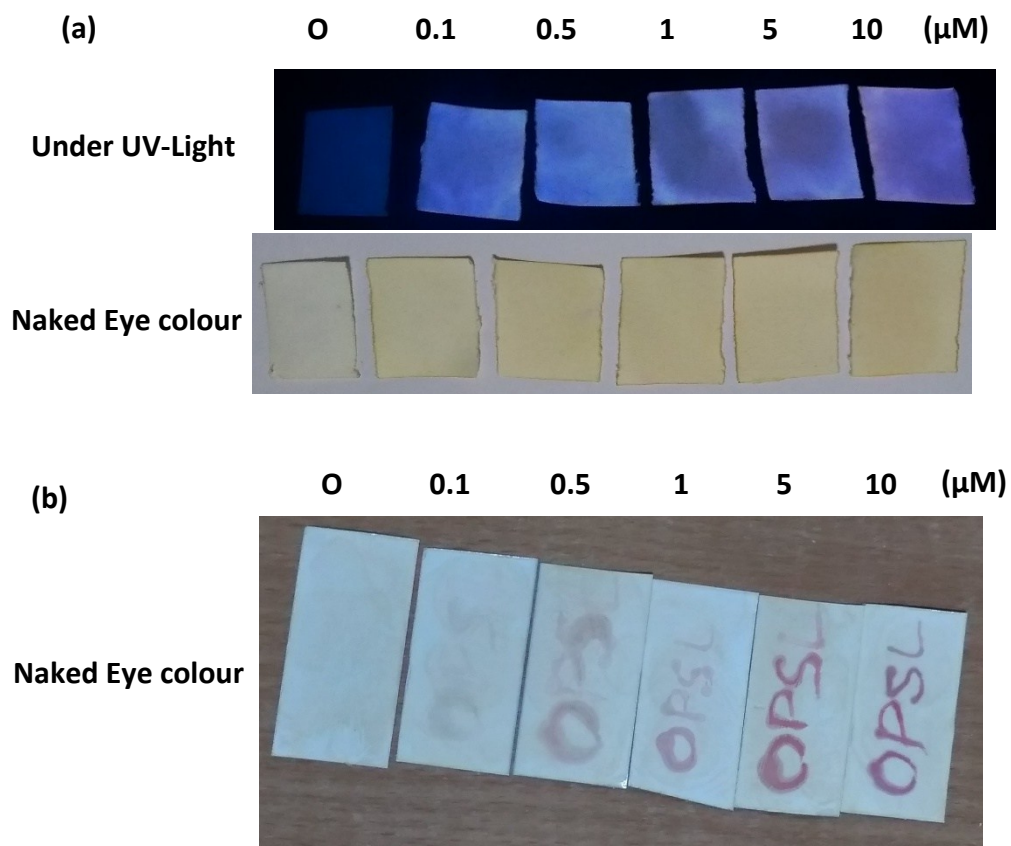
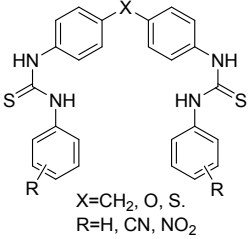
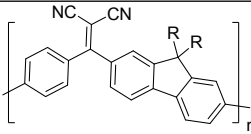
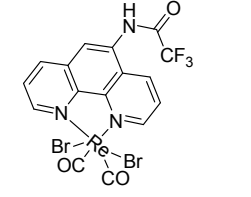
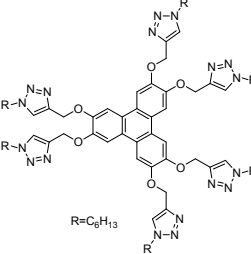
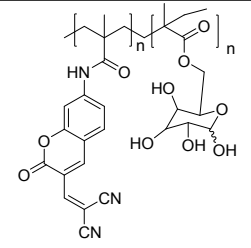
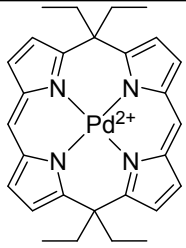
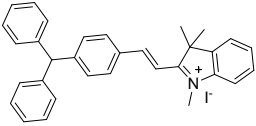
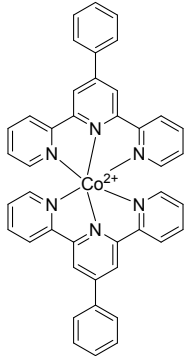
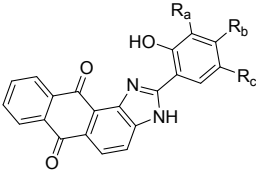
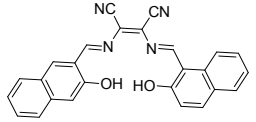
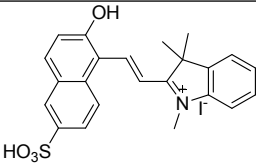
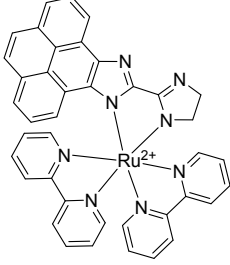
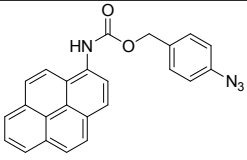
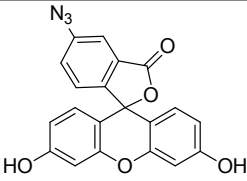
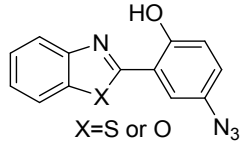
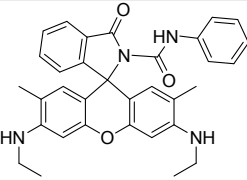
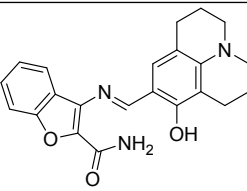
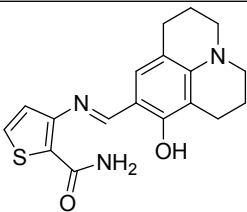
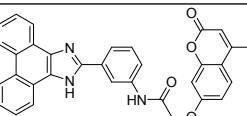


Fig. 14: Strip Test for CN^- (a) Under UV-Light and naked eye response of the probe R with various concentration of CN^- ranging from (0.1-10) μM ; Strip test for H_2S (b) Naked eye response of the probe R with various concentration of H_2S ranging from (0.1-10) μM .

Table S1: Comparison table of the reported receptors for CN^- , Fe^{3+} , and H_2S .

Ref. No.	Molecular Structure	Analytes	Detection limit	Solvent	Sensing Mode	Application
1.	 <p>X=CH₂, O, S. R=H, CN, NO₂</p>	CN^-	3.7 μM	THF-DMSO (99:1)	Deprotonation	KCN in Water
2.		CN^-	14 nM	DMF	Nucleophilic Reaction	—
3.		CN^-	—	ACN	Deprotonation	—
4.	 <p>R=C₆H₁₃</p>	Cu^{2+} and CN^-	3.12 μM (Cu^{2+}), 2.5 μM (CN^-)	DMSO	Complexation	TLC strip test
6.		CN^-	1.17 μM	HEPES buffered Water	Nucleophilic Reaction	—

7.		CN ⁻	0.3 μM	ACN	Nucleophilic Reaction	_____
8.		CN ⁻	21 nM	EtOH-Tris HCl buffer (4:6)	Nucleophilic Reaction	strip test
9.		CN ⁻	10 μM	MeOH- Water	Redox Reaction	_____
10.	 R1 => Ra, Rc=H, Rb=OH R2 => Ra, Rc=t-Bu, Rb=H	CN ⁻	0.53 μM	Water- DMSO (6:4)	Deprotonation	CN ⁻ in Waste Water
12.		CN ⁻	—	DMSO- Water (7:3)	Deprotonation	Strip test
14.		CN ⁻	0.021 μM	THF	Nucleophilic Reaction	Bio Imaging

18.		CN ⁻	5.24 nM	DMSO	Deprotonation	_____
15.		H ₂ S	158 nM	Water-DMSO (20:80)	Reduction Reaction	Bio Imaging
16.		H ₂ S and NO	2.6 μM and 0.12 μM	MeOH/Glycerin	Reduction Reaction	Bio Imaging
17.		H ₂ S	_____	EtOH/PBS Buffer (1:1)	Reduction Reaction	Bio Imaging
20.		Fe ³⁺ and Acetate	0.18 μM (Acetate)	Water-CAN (1:1)	Reversible Ring Opening	_____
22		Fe ²⁺ / Fe ³⁺ and PPI	0.36 and 0.37 μM	DMSO	Complexation	_____
23.		Fe ³⁺ / PPI	1.15 μM	Bis-Tris Buffer	Complexation	_____
24.		Fe ³⁺ / PPI	4.8 μM	DMF/HEPES	Complexation	Real Sample water

26.		Fe ³⁺	6.6 μM	ACN/HEPES	Reversible Ring Opening	Real Sample
27.		Fe ³⁺	0.025 μM	EtOH/Water (1:1)	Reversible Ring Opening	Bio Imaging
28.		Cu ²⁺ / Fe ³⁺	0.98 μM (Cu ²⁺) and 9.5 μM (Fe ³⁺)	ACN	Complexation	_____
34.		Fe ³⁺ / PPI	87.3 nM and 12.5 nM	DMSO: Water (3:7)	Complexation	Bio Imaging
37.		Fe ³⁺ -CN ⁻ (Relay Recognition)	0.2 μM (Fe ³⁺) and 0.26 nM (CN ⁻)	Water:DMSO (1:1)	Complexation	Strip test

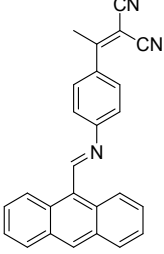
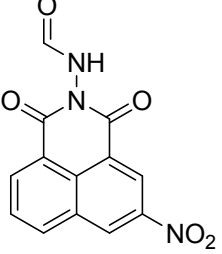
38.		CN ⁻ - Fe ³⁺ (Relay Recognition)	8.11 μM (CN ⁻)	ACN	Nucleophilic Reaction	Bio Imaging
This Work		CN ⁻ /Fe ³⁺ (Relay Recognition) and H ₂ S	17.5 nM (CN ⁻), 8.69 μM (Fe ³⁺) and 8.1 μM (H ₂ S)	Water:DMSO (1:9)	Reversible protonation (CN ⁻ /Fe ³⁺) and nitro group reduction (H ₂ S)	Strip Test, Bio imaging and Zebrafish Imaging.

Table S2: Quantum Yield of the CN⁻/Fe³⁺ relay sensing process.

Sl. No.	Species	Absorption Maxima	Absorbance	Emission Area	Quantum Yield (ϕ)
1.	Receptor	283	0.6756	16836	0.015
2.	Receptor+CN ⁻	530	0.2316	331925	0.86
3.	Receptor+CN ⁻ +Fe ³⁺	530	0.1	2038	0.013
4.	Rhodamine B	564	0.2573	406254	0.95